A Novel Subspace-Aided Fault Detection Approach for the Drive Systems of Rolling Mills

Mingyi Huo, *Student Member, IEEE*, Hao Luo, *Senior Member, IEEE*, Shen Yin, *Senior Member, IEEE*, Yuchen Jiang, *Student Member, IEEE*, and Okyay Kaynak, *Life Fellow, IEEE*

***Abstract*— This brief proposes a subspace-aided fault detection approach for the drive systems of strip rolling mills. Considering the impact of the unknown periodic load generated by the strip rolling process, the primary contributions are concluded as follows. First, this brief presents an approach to describe the subspace of the unknown/unmeasurable periodic load. Second, a fundamental frequency identification approach for the drive systems is proposed and then the subspace of the unknown periodic load can be constructed by the fundamental frequency. Third, this brief presents a subspace-aided fault detection approach to identify the data-driven stable kernel representation (SKR) of the closed-loop system by projecting the input–output (I/O) process data, so as to obtain a robust residual against the unknown periodic load. In addition, the effectiveness and performance of the approaches are verified by numerical examples and experimental data of the test rig for the drive systems of strip rolling mills. The results show that a robust residual generation against the unknown periodic load in the drive systems can be obtained and the robust subspace-aided fault detection can be achieved. Compared with the traditional method, the proposed approaches can improve the fault detection rate more effectively and be applied to the drive systems of strip rolling mills reliably.**

***Index Terms*— Data-driven, data-driven stable kernel representation (SKR), fault detection, industrial rolling mill drive system, periodic load, subspace.**

I. Introduction

With the development of industrial production technology, the operating conditions of modern production systems have become more complex. Complex data make it difficult to identify the operation state of industrial systems directly. To ensure the safety and reliability of systems, it is necessary to do fault detection category research [1], [2]. Various fault detection methods have been basically covered in industrial applications, such as plant-wide process [3], high-speed train [4]–[8], and most techniques and applications of fault detection are summarized in [9].

The data-driven scheme has been developed in [10] and further studied in [11] and [12]. Yin *et al.* [13] propose multivariate statistical analysis and optimization process monitoring methods for data-driven fault detection. Luo *et al.* [14] analyze the robustness of systems in this data-driven framework. In the field of data-driven fault detection, subspace identification technology has attracted more and more attention over the past decades, focusing on dynamic processes. In this way, without knowing the model of a system, the stable kernel representation (SKR) of the system which forms the residual generator can be identified. These subspace identification methods have been well verified in the numerical examples of industrial systems. However, as the disturbance is inevitable in the operating state of systems, the results of process monitoring fault detection in the practical applications are unsatisfactory. The disturbance needs to be considered in practical application.

In recent years, the subspace-aided fault detection approaches considering known/measurable disturbance have drawn extensive attention [15], [16]. A subspace-aided fault detection method is presented [17] to solve the problem of roll eccentricity. However, the traditional subspace identification approach is not ideal, and the disturbance cannot be measured in practice, so the fault detection technology with unknown disturbance is still a common problem. Different from [17], based on the previous research [18], this brief takes into account the impact of unknown periodic load generated by the strip rolling process and proposes a subspace fault detection approach for the drive systems of strip rolling mill, which is verified by the actual experimental data. The contributions are described as follows.

1) This brief proposes a fundamental frequency identification approach in Section III-C, which sets the stage for the subsequent contributions.
2) In Section III-B, it presents a signal subspace description approach for unknown periodic load in the drive systems of rolling mills generated by the roll bite area. The subspace can be constructed by the fundamental frequency which is identified by the first contribution.
3) The subspace identification of the data-driven SKR with unknown periodic load is studied for the drive systems of rolling mills in Section IV, which is realized by

Manuscript received April 18, 2021; accepted August 12, 2021. Manuscript received in final form August 28, 2021. This work was supported in part by the National Natural Science Foundation of China (NSFC) under Grant 62073104 and Grant 61703121. Recommended by Associate Editor P. F. F. Odgaard. *(Corresponding author: Hao Luo.)*

Mingyi Huo, Hao Luo, and Yuchen Jiang are with the Department of Control Science and Engineering, Harbin Institute of Technology, Harbin 150001, China (e-mail: mingyihuo111@163.com; hao.luo@hit.edu.cn; yc.jiang2016@foxmail.com).

Shen Yin is with the Department of Mechanical and Industrial Engineering, Faculty of Engineering, Norwegian University of Science and Technology, 7033 Trondheim, Norway (e-mail: shen.yin@ntnu.no).

Okyay Kaynak is with the Department of Electrical and Electronics Engineering, Boğaziçi University, 34342 Istanbul, Turkey, and also with the School of Automation and Electrical Engineering and the Institute of Artificial Intelligence, University of Science and Technology Beijing, Beijing 100083, China (e-mail: okyay.kaynak@boun.edu.tr).

Color versions of one or more figures in this article are available at https://doi.org/10.1109/TCST.2021.3109051.

Digital Object Identifier 10.1109/TCST.2021.3109051

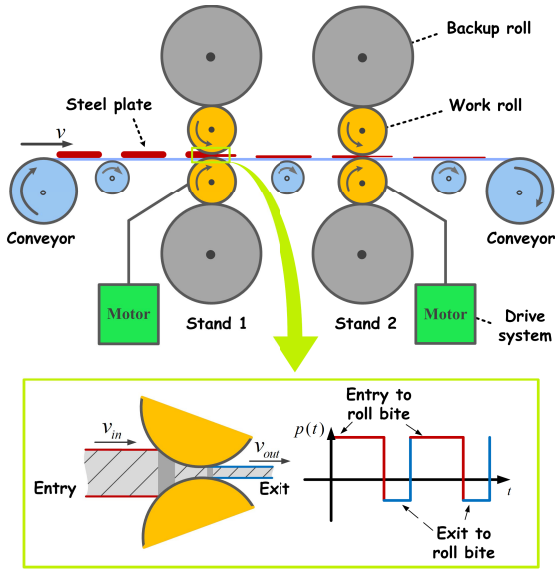

Fig. 1. Strip rolling mill configuration.

projecting the process data into the different subspaces. As a result, a robust residual generation against the unknown periodic load in the drive system can be obtained to achieve better fault detection.

The following is the structure of this brief. The problem formulation of the strip rolling process is given in Section II. Then, it presents the subspace description of unknown periodic load and a fundamental frequency identification approach in Section III. A data-driven SKR with the unknown periodic load is identified by the subspace identification method in Section IV. In Section V, the benchmark study is performed that includes numerical simulation and experimental verification. In the end, the conclusion is given in Section VI.

II. Strip Rolling Process and Problem Formulation

A. Strip Rolling Process

Strip rolling is a process of converting raw materials into finished products. The thickness of the steel plate is reduced during rolling. The steel plate is first heated in the furnace and then rolled into coils for further processing.

A typical mill-stand arrangement and the whole strip rolling process are briefly described as shown in Fig. 1. Taking a four-high roll in a typical stand-alone two-stand rolling mill, the steel plate passes through two separate pairs of work rolls which are supported by the backup rolls. The work rolls are directly in contact with the plate and are powered by the drive systems of rolling mills such as electric motors, in general.

The reduction in thickness is due to high pressure in a small area between the work rolls called the roll bite area [19]. The bite area begins when the head of the steel plate almost touches the work rolls and terminates when the tail of the steel plate is almost away from the work rolls. Therefore, the whole process in the bite area will be divided into two parts: the entry and exit of bite. Correspondingly, the plates are also classified as incoming plates and exiting plates. Referring to Fig. 1, the steel plate will enter the bite area at v_{in} speed and exit the bite area at v_{out} speed. As a result, all steel plates are passed one by one between the work rolls, which generates a set of loads similar to the pulse waveform in Fig. 1, where $p(t)$ denotes the function of the periodic pulse wave.

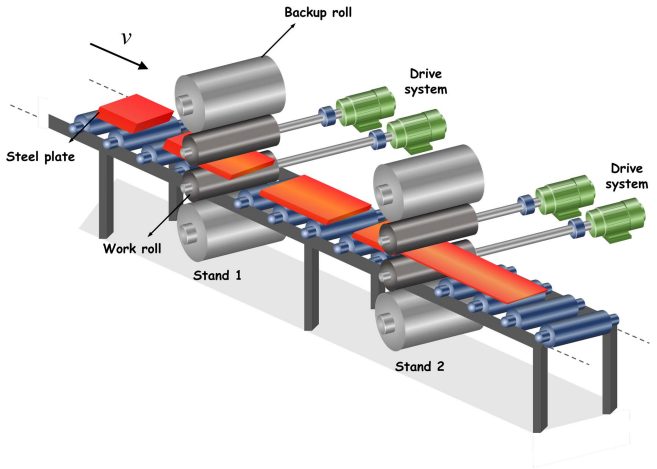

Fig. 2. Schematic of the impact of periodic load on the speed of drive systems.

Due to the high bearing force, the deformation of the steel plate causes an abnormal speed variation of the work rolls. As each steel plate passes through, the motor drive is in a cycle from load to no-load as shown in Fig. 2. Under this load, the drive system of the rolling mill is easy to go wrong. If the periodic load in the rolling process is not considered, once the drive system is in the faulty condition, the fault signal cannot be separated from the periodic load and is easily submerged in the periodic load, so it cannot be detected in time, which may cause significant industrial accidents. Therefore, it is important to study fault detection of drive systems in the rolling process. In this brief, a fault detection approach for the drive systems of rolling mills under periodic load is studied. It is devoted to accurately and timely monitoring the drive system of rolling mills under periodic load situations.

B. Problem Formulation

The dynamic performance of the drive systems studied in this brief is evaluated in a dynamic discrete-time system, which is simplified as linear time-invariant (LTI) in terms of closing to the working point. The nonlinearity case [20] is beyond the scope of this brief. A drive system $\mathbf{G}(z)$ of the strip rolling mill can be described as

$$\mathbf{y}(z) = \mathbf{G}(z)\mathbf{u}(z) + \mathbf{d}(z) + \boldsymbol{\alpha}(z) \tag{1}$$

where $\mathbf{u}(z) \in \mathcal{R}^l$ and $\mathbf{y}(z) \in \mathcal{R}^m$ are input vector and output vector, respectively. The vector $\boldsymbol{\alpha}(z) \in \mathcal{R}^{n_a}$ is unknown noise sequence, which is independent of the input vector $\mathbf{u}(z)$. $\mathbf{d}(z)$ is the periodic load sequence affecting the drive system generated by the roll bite area. The state-space representation is another description which takes the form

$$\mathbf{x}_{k+1} = \mathbf{A}\mathbf{x}_k + \mathbf{B}\mathbf{u}_k + \mathbf{E}_\mathbf{d}\mathbf{d}_k + \mathbf{E}_{\boldsymbol{\alpha}}\boldsymbol{\alpha}_k \tag{2}$$

$$\mathbf{y}_k = \mathbf{C}\mathbf{x}_k + \mathbf{D}\mathbf{u}_k + \mathbf{F}_\mathbf{d}\mathbf{d}_k + \mathbf{F}_{\boldsymbol{\alpha}}\boldsymbol{\alpha}_k \tag{3}$$

where $\mathbf{x}_k \in \mathcal{R}^{n_x}$ denotes the state, $\boldsymbol{\alpha}_k$ is the noise vector, and $\mathbf{d}_k$ represents the periodic load vector.

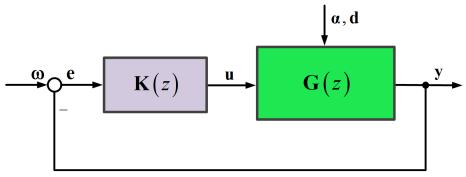

Fig. 3. Feedback control diagram.

The feedback control diagram of the drive systems is shown as Fig. 3. The general feedback controller $\mathbf{K}(z)$ has the following state-space realization:

$$\mathbf{x}_{\mathbf{c},k+1} = \mathbf{A}_\mathbf{c}\mathbf{x}_{\mathbf{c},k} + \mathbf{B}_\mathbf{c}(\boldsymbol{\omega}_k - \mathbf{y}_k) \tag{4}$$

$$\mathbf{u}_k = \mathbf{C}_\mathbf{c}\mathbf{x}_{\mathbf{c},k} + \mathbf{D}_\mathbf{c}(\boldsymbol{\omega}_k - \mathbf{y}_k) \tag{5}$$

where the tracking reference $\boldsymbol{\omega}_k$ is uncorrelated with the system's unknown noise sequence. Following are the assumptions of feedback control structure.

1) The closed-loop in Fig. 3 is internally stabilized by the feedback controller $\mathbf{K}(z)$.
2) The tracking reference $\boldsymbol{\omega}_k \in \mathcal{R}^m$ is independent of the noise $\boldsymbol{\alpha}_k \in \mathcal{R}^{n_\alpha}$ and satisfies the persistent excitation condition.
3) The state vector $\mathbf{x}_k \in \mathcal{R}^{n_x}$ is fully excited, and it has enough measurements $\boldsymbol{\omega}_k$, $\mathbf{u}_k$, and $\mathbf{y}_k$ available.

According to the definition of the left coprime factorizations [21] of $\mathbf{G}(z)$ and the data-driven SKR [11], the residual generator $\mathbf{r}_k$ can be denoted as follows, which includes the unknown periodic load and noise:

$$\mathbf{r}_k = \mathcal{K}_{\mathbf{d},\mathbf{s}}\begin{bmatrix}\mathbf{u}_{\mathbf{s},\mathbf{k}}\\ \mathbf{y}_{\mathbf{s},\mathbf{k}}\end{bmatrix} = \text{unknown periodic load} + \text{noise}$$

where the full-row rank matrix $\mathcal{K}_{\mathbf{d},\mathbf{s}} \in \mathcal{R}^{n_\mathcal{K} \times s(l+m)}$ is the data-driven SKR, $\mathbf{u}_{\mathbf{s},\mathbf{k}}$ and $\mathbf{y}_{\mathbf{s},\mathbf{k}}$ represent the stacked data vectors of length s as follows:

$$\mathbf{u}_{\mathbf{s},\mathbf{k}} = \begin{bmatrix}\mathbf{u}_k\\ \vdots\\ \mathbf{u}_{k+s-1}\end{bmatrix} \in \mathcal{R}^{\text{sl}}, \quad \mathbf{y}_{\mathbf{s},\mathbf{k}} = \begin{bmatrix}\mathbf{y}_k\\ \vdots\\ \mathbf{y}_{k+s-1}\end{bmatrix} \in \mathcal{R}^{\text{sm}}. \tag{6}$$

III. Subspace Description of the Unknown Periodic Load in the Drive Systems

In the strip rolling process, it is difficult to measure the load. To solve this problem, a subspace description approach is proposed which can accurately simulate the real load generated by the strip rolling process. The periodic load in the drive systems of strip rolling mills could be considered as a periodic pulse wave [22].

A. Fourier Series of Periodic Pulse Wave

For a continuous-time period signal $f(t)$, the Fourier series expansion can be described as

$$f(t) = \sum_{n=-\infty}^{\infty} c_n e^{\text{in}\omega_0 t} = c_0 + \sum_{n=1}^{\infty}\left(c_n e^{\text{in}\omega_0 t} + c_{-n}e^{-\text{in}\omega_0 t}\right)$$

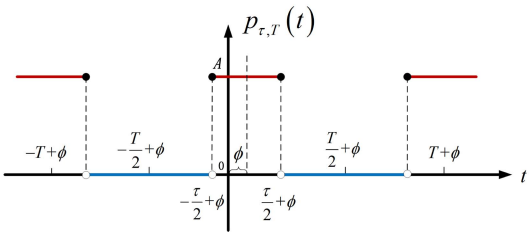

Fig. 4. Periodic pulse wave function $p_{\tau,T}(t)$.

where the fundamental frequency $\omega_0 = 2\pi/T$, with T being the period of the signal. The component signals with different values of n have harmonic relationships, and the frequencies of the component functions are all integer multiples of fundamental frequency. c_0 and c_n are the complex Fourier coefficients of $f(t)$, which have the following form [23]:

$$c_n = \frac{1}{T}\int_{t_0}^{T+t_0} f(t)e^{-\text{in}\omega_0 t}dt, \quad \text{for } n \in \mathbb{Z}.$$

Consider a periodic pulse wave function $p_{\tau,T}(t)$ with an amplitude of A, then the complex Fourier coefficients become

$$c_0 = \frac{A\tau}{T}, \quad c_n = c_{-n} = \frac{2A}{T}\cdot\frac{\sin(n\omega_0\tau/2)}{n\omega_0}$$

where τ is the pulse time, and τ/T and ϕ denote the duty cycle and the phase offset, respectively.

Therefore, an ideal periodic pulse wave in Fig. 4 can be described as follows, which is composed of a series of cosine waves:

$$p_{\tau,T}(t) = \frac{A\tau}{T} + \sum_{n=1}^{\infty}\frac{2A}{n\pi}\cdot\sin\left(\frac{\pi\tau n}{T}\right)\cdot\cos(n\omega_0(t-\phi)).$$

B. Subspace Description

In this brief, it is necessary to discuss the number of cosine waves in order to accurately describe the subspace of the unknown periodic load in this brief. Therefore, the unknown periodic load in the drive systems is expressed as the sum of finite cosine waves

$$\begin{aligned}\mathbf{d}_k &= \frac{A\tau}{T} + \sum_{n=1}^{n_f}\frac{2A}{n\pi}\cdot\sin\left(\frac{\pi\tau n}{T}\right)\cdot\cos(n\omega_0(kt_s-\phi))\\ &= \mathcal{C} + \sum_{n=1}^{n_f} a_n\cos(\omega_n k t_s + \varphi_n)\end{aligned} \tag{7}$$

where $\mathcal{C}$, ω_n, a_n, and φ_n denote the bias, frequency, amplitude, and phase of the nth cosine wave component, respectively. n is the integer multiple of the fundamental frequency in the series of cosine waves, n_f not only ensures the accuracy of the subspace of the unknown periodic load, but also consider the computational complexity. The integer k is the discrete-time sampling points. t_s denotes the sampling period which satisfies the Nyquist–Shannon sampling theorem, that is, $t_s \geq \pi/(n\omega_0)$, and therefore, the integer multiple of the fundamental frequency should be $n \leq \pi/(\omega_0 t_s)$.

In (7), since the following trigonometric identity holds:

$$a_n\cos(\omega_n k + \varphi_n) = \beta_{n,1}\sin(\omega_n k) + \beta_{n,2}\cos(\omega_n k) \tag{8}$$

Algorithm 1 Subspace Description of the Unknown Periodic Load

S1: Rewrite the periodic load $\mathbf{d}_k$ as Eq.(9).
S2: Construct periodic load vector $\mathbf{d}_{\mathbf{s},\mathbf{k}}$ as Eq.(10).
S3: Then, the unknown periodic load in the drive systems can be described as a Hankel matrix $\mathbf{D}_{\mathbf{k},\mathbf{s},\mathbf{N}}$.
S4: Thus, the subspace of the unknown periodic load $\mathbf{D}_{\mathbf{b},\mathbf{N}}$ can be obtained.

in which

$$\beta_{n,1} = -a_n \sin(\varphi_n), \quad \beta_{n,2} = a_n \cos(\varphi_n)$$

the periodic load $\mathbf{d}_k$ in (7) can be rewritten as follows:

$$\mathbf{d}_k = \mathbf{P} \cdot \boldsymbol{\rho}_k \tag{9}$$

where $\mathbf{P}$ contains the bias, amplitude, phase, and duty cycle, and $\boldsymbol{\rho}_k$ includes frequencies

$$\mathbf{P} = \left[\mathcal{C}\ \beta_{1,1}\ \beta_{1,2},\ \ldots,\ \beta_{n,1}\ \beta_{n,2}\right]$$
$$\boldsymbol{\rho}_k = \left[1\ \sin(\omega_1 k)\ \cos(\omega_1 k),\ \ldots,\ \sin(\omega_n k)\ \cos(\omega_n k)\right]^T.$$

Then, a data vector $\mathbf{d}_{\mathbf{s},\mathbf{k}}$ of length s is presented

$$\mathbf{d}_{\mathbf{s},\mathbf{k}} = \begin{bmatrix} \mathbf{d}_k \\ \mathbf{d}_{k+1} \\ \vdots \\ \mathbf{d}_{k+s-1} \end{bmatrix} = \begin{bmatrix} \mathbf{P}\boldsymbol{\rho}_k \\ \mathbf{P}\boldsymbol{\rho}_{k+1} \\ \vdots \\ \mathbf{P}\boldsymbol{\rho}_{k+s-1} \end{bmatrix} = \underbrace{\begin{bmatrix} \mathbf{P} \\ \mathbf{PT} \\ \vdots \\ \mathbf{PT}^{s-1} \end{bmatrix}}_{\mathbf{P_s}} \boldsymbol{\rho}_k. \tag{10}$$

where $\mathbf{T}$ is the diagonal matrix that contains the rotation invertible matrices. The detailed derivation and the Hankel matrix form are shown in the previous research in [17] which are not be covered again here. Therefore, the unknown periodic load in the drive systems can be described as the following Hankel matrix. *(For the construction of the Hankel matrix, see the reference [12], and so on.)*

$$\mathbf{D}_{\mathbf{k},\mathbf{s},\mathbf{N}} = \left[\mathbf{d}_{\mathbf{s},\mathbf{k}}\ \mathbf{d}_{\mathbf{s},\mathbf{k+1}}\ \ldots\ \mathbf{d}_{\mathbf{s},\mathbf{k+N-1}}\right] = \mathbf{P_s}\mathbf{D}_{\mathbf{b},\mathbf{N}} \tag{11}$$

where $\mathbf{D}_{\mathbf{b},\mathbf{N}} = \left[\boldsymbol{\rho}_k\ \boldsymbol{\rho}_{k+1}\ \ldots\ \boldsymbol{\rho}_{k+N-1}\right] \in \mathcal{R}^{(2n_f+1)\times N}$ is the subspace description of the unknown periodic load. $\boldsymbol{\rho}_k$ holds a matrix of sines and cosines with different multiples of fundamental frequency ω_0.

The subspace description method is summarized in the following algorithm. In order to verify the accuracy of the algorithm, the similarity between the real pulse wave and the subspace description $\mathbf{D}_{\mathbf{b},\mathbf{N}}$ is tested, so as to provide guidance for selecting the appropriate n_f. More details will be presented in Section V-A.

C. Fundamental Frequency Identification

It is necessary to require a given fundamental frequency to describe the subspace $\mathbf{D}_{\mathbf{b},\mathbf{N}}$, so a fundamental frequency identification method is proposed in this section.

The unknown periodic load in the drive systems with noise can be expressed as

$$\mathbf{d}_k = \mathcal{C} + \sum_{n=1}^{n_f} a_n \cos(\omega_n k t_s + \varphi_n) + \mathbf{v}_k. \tag{12}$$

According to the formulas of trigonometric functions based on Chebyshev method, it yields

$$\cos(\omega k) = 2\cos(\omega)\cos(\omega(k-1)) - \cos(\omega(k-2))$$
$$\sin(\omega k) = 2\cos(\omega)\sin(\omega(k-1)) - \sin(\omega(k-2))$$

that is,

$$\begin{bmatrix} \cos(\omega(k-1)) \\ \cos(\omega k) \end{bmatrix} = \begin{bmatrix} 0 & 1 \\ -1 & 2\cos(\omega) \end{bmatrix} \begin{bmatrix} \cos(\omega(k-2)) \\ \cos(\omega(k-1)) \end{bmatrix}$$
$$\begin{bmatrix} \sin(\omega(k-1)) \\ \sin(\omega k) \end{bmatrix} = \begin{bmatrix} 0 & 1 \\ -1 & 2\cos(\omega) \end{bmatrix} \begin{bmatrix} \sin(\omega(k-2)) \\ \sin(\omega(k-1)) \end{bmatrix}$$

then the nth component of the periodic load $\mathbf{d}_k$ can be denoted by the second-order dynamic system

$$\mathbf{x}_{\mathbf{d}n,k+1} = \mathbf{A}_{\mathbf{d}n}\mathbf{x}_{\mathbf{d}n,k},\ \mathbf{x}_{\mathbf{d}n,0} \tag{13}$$
$$\mathbf{d}_{n,k} = \mathbf{C}_{\mathbf{d}n}\mathbf{x}_{\mathbf{d}n,k} \tag{14}$$

where

$$\mathbf{A}_{\mathbf{d}n} = \begin{bmatrix} 0 & 1 \\ -1 & 2\cos(nt_s\omega_0) \end{bmatrix}, \mathbf{C}_{\mathbf{d}n} = \begin{bmatrix} 0 & 1 \end{bmatrix}$$
$$\mathbf{x}_{\mathbf{d}n,k} = \begin{bmatrix} \alpha_n \cos((k-1)nt_s\omega_0 + \varphi_n) \\ \alpha_n \cos(knt_s\omega_0 + \varphi_n) \end{bmatrix}$$
$$\mathbf{x}_{\mathbf{d}n,k+1} = \begin{bmatrix} \alpha_n \cos(knt_s\omega_0 + \varphi_n) \\ \alpha_n \cos((k+1)nt_s\omega_0 + \varphi_n) \end{bmatrix}.$$

Therefore, the periodic load $\mathbf{d}_k$ in (12) can be formulated as

$$\mathbf{x}_{\mathbf{d}k+1} = \mathbf{A}_{\mathbf{d}}\mathbf{x}_{\mathbf{d}k} \tag{15}$$
$$\mathbf{d}_k = \mathcal{C} + \mathbf{C}_{\mathbf{d}}\mathbf{x}_{\mathbf{d}k} + \mathbf{v}_k \tag{16}$$

where

$$\mathbf{A}_{\mathbf{d}} = \begin{bmatrix} \mathbf{A}_{\mathbf{d}1} & \cdots & \mathbf{0} & \cdots & \mathbf{0} \\ \vdots & \ddots & \vdots & \ddots & \vdots \\ \mathbf{0} & \cdots & \mathbf{A}_{\mathbf{d}n} & \cdots & \mathbf{0} \\ \vdots & \ddots & \vdots & \ddots & \vdots \\ \mathbf{0} & \cdots & \mathbf{0} & \cdots & \mathbf{A}_{\mathbf{d}n_f} \end{bmatrix}, \mathbf{x}_{\mathbf{d}0} = \begin{bmatrix} \mathbf{x}_{\mathbf{d}1,0} \\ \vdots \\ \mathbf{x}_{\mathbf{d}n,0} \\ \vdots \\ \mathbf{x}_{\mathbf{d}n_f,0} \end{bmatrix}$$
$$\mathbf{C}_{\mathbf{d}} = \begin{bmatrix} \mathbf{C}_{\mathbf{d}1} & \cdots & \mathbf{C}_{\mathbf{d}n} & \cdots & \mathbf{C}_{\mathbf{d}n_f} \end{bmatrix}$$
$$\mathbf{x}_{\mathbf{d}k} = \begin{bmatrix} \mathbf{x}_{\mathbf{d}1,k} & \cdots & \mathbf{x}_{\mathbf{d}n,k} & \cdots & \mathbf{x}_{\mathbf{d}n_f,k} \end{bmatrix}^T$$
$$\mathbf{x}_{\mathbf{d}k+1} = \begin{bmatrix} \mathbf{x}_{\mathbf{d}1,k+1} & \cdots & \mathbf{x}_{\mathbf{d}n,k+1} & \cdots & \mathbf{x}_{\mathbf{d}n_f,k+1} \end{bmatrix}^T.$$

Since the eigenvalues of $\mathbf{A}_{\mathbf{d}n}$ are

$$\lambda_n = \cos(nt_s\omega_0) + j\sin(nt_s\omega_0) \tag{17}$$

where λ_n represents the eigenvalues of $\mathbf{A}_{\mathbf{d}n}$ for the imaginary number. Then, the problem of frequency estimation in (12) is reduced to the eigenvalue identification problem of system matrix $\mathbf{A}_{\mathbf{d}}$ in the dynamic system (15) and (16), that is,

$$\omega_0 = \frac{1}{nt_s}\arccos(\mathrm{Re}(\lambda_n)) \tag{18}$$

where $\mathrm{Re}(\cdot)$ represents the real part of a complex number. Then, a fundamental frequency identification approach is presented.

The periodic load $\mathbf{d}_k$ in (12) can be reformulated into following stacked data vectors by $s_{\rm dp}$ and $s_{\rm df}$:

$$\mathbf{d}_{\mathbf{s_{dp}},\mathbf{k}-\mathbf{s_{dp}}} = \begin{bmatrix} \mathbf{d}_{k-s_{\rm dp}} \\ \vdots \\ \mathbf{d}_{k-1} \end{bmatrix} \in \mathcal{R}^{s_{\rm dp}}, \mathbf{d}_{\mathbf{s_{df}},\mathbf{k}} = \begin{bmatrix} \mathbf{d}_{k} \\ \vdots \\ \mathbf{d}_{k+s_{\rm df}-1} \end{bmatrix} \in \mathcal{R}^{s_{\rm df}}.$$

After N times of the truncations from truncating instant k to $k+N-1$, the following Hankel matrices are constructed:

$$\mathbf{D}_{\mathbf{s_{dp}},\mathbf{N}} = \begin{bmatrix} \mathbf{d}_{\mathbf{s_{dp}},\mathbf{k}-\mathbf{s_{dp}}} & \cdots & \mathbf{d}_{\mathbf{s_{dp}},\mathbf{k}-\mathbf{s_{dp}}+\mathbf{N}-1} \end{bmatrix} \in \mathcal{R}^{s_{\rm dp}\times N}$$
$$\mathbf{D}_{\mathbf{s_{df}},\mathbf{N}} = \begin{bmatrix} \mathbf{d}_{\mathbf{s_{df}},\mathbf{k}} & \cdots & \mathbf{d}_{\mathbf{s_{df}},\mathbf{k}+\mathbf{N}-1} \end{bmatrix} \in \mathcal{R}^{s_{\rm df}\times N}.$$

Then, the state-space realization

$$\mathbf{D}_{\mathbf{s_{df}},\mathbf{N}} = \boldsymbol{\mathcal{C}}_{\mathbf{s_{df}},\mathbf{N}} + \boldsymbol{\Gamma}_{\mathbf{s_{df}}}\mathbf{X}_{\mathbf{dk},\mathbf{1},\mathbf{N}} + \mathbf{V}_{\mathbf{s_{df}},\mathbf{N}} \tag{19}$$

where $\mathbf{X}_{\mathbf{dk},\mathbf{1},\mathbf{N}} = [\,\mathbf{x}_{\mathbf{d}k}\ \cdots\ \mathbf{x}_{\mathbf{d}k+N-1}\,] \in \mathcal{R}^{2n_f\times N}$, $\boldsymbol{\mathcal{C}}_{\mathbf{s_{df}},\mathbf{N}}$ is the duty cycle term, $\mathbf{V}_{\mathbf{s_{df}},\mathbf{N}}$ represents the noise term in $\mathbf{D}_{\mathbf{s_{df}},\mathbf{N}}$ which is constructed by $\mathbf{v}_k$, $\boldsymbol{\Gamma}_{\mathbf{s_{df}}}$ is an extended observability matrix of full-column rank form

$$\boldsymbol{\Gamma}_{\mathbf{s_{df}}} = \begin{bmatrix} \mathbf{C_d} \\ \mathbf{C_dA_d} \\ \vdots \\ \mathbf{C_dA_d}^{s_{\rm df}-1} \end{bmatrix} \in \mathcal{R}^{s_{\rm df}\times 2n_f}.$$

Assume that the noise sequence $\mathbf{v}_k$ is white zero-mean and independent of the initial state vector $\mathbf{x}_{\mathbf{d}0}$, then perform the following LQ decomposition:

$$\begin{bmatrix} \mathbf{T_c} \\ \mathbf{D}_{\mathbf{s_{dp}},\mathbf{N}} \\ \mathbf{D}_{\mathbf{s_{df}},\mathbf{N}} \end{bmatrix} = \begin{bmatrix} \mathbf{L_{d11}} & \mathbf{0} & \mathbf{0} \\ \mathbf{L_{d21}} & \mathbf{L_{d22}} & \mathbf{0} \\ \mathbf{L_{d31}} & \mathbf{L_{d32}} & \mathbf{L_{d33}} \end{bmatrix} \begin{bmatrix} \mathbf{Q_{d1}} \\ \mathbf{Q_{d2}} \\ \mathbf{Q_{d3}} \end{bmatrix} \tag{20}$$

where $\mathbf{T_c} = [\,1\ 1\ \cdots\ 1\ 1\,] \in \mathcal{R}^N$ represents the duty cycle subspace of the periodic load. It leads to $\mathbf{V}_{\mathbf{s_{df}},\mathbf{N}} = \mathbf{L_{d33}Q_{d3}}$, and thus it holds

$$\boldsymbol{\Gamma}_{\mathbf{s_{df}}}\mathbf{X}_{\mathbf{dk},\mathbf{1},\mathbf{N}} = \mathbf{L_{d32}Q_{d2}}. \tag{21}$$

Then, perform the singular value decomposition (SVD) on $\mathbf{L_{d32}Q_{d2}}$

$$\mathbf{L_{d32}Q_{d2}} = \underbrace{\begin{bmatrix} \mathbf{U_1} & \mathbf{U_2} \end{bmatrix}}_{\mathbf{U}} \underbrace{\begin{bmatrix} \boldsymbol{\Sigma}_1 & \mathbf{0} \\ \mathbf{0} & \boldsymbol{\Sigma}_2 \approx \mathbf{0} \end{bmatrix}}_{\boldsymbol{\Sigma}} \underbrace{\begin{bmatrix} \mathbf{V_1}^T \\ \mathbf{V_2}^T \end{bmatrix}}_{\mathbf{V}^T}. \tag{22}$$

$\boldsymbol{\Gamma}_{\mathbf{s_{df}}}$ can be determined as

$$\boldsymbol{\Gamma}_{\mathbf{s_{df}}} = \mathbf{U_1}\boldsymbol{\Sigma}_{\mathbf{1}}^{1/2}. \tag{23}$$

Then, $\mathbf{A_d}$ can be identified as

$$\mathbf{A_d} = \boldsymbol{\Gamma}^{\dagger}_{\mathbf{s_{df}},\mathbf{1}:\mathbf{s_{df}}-\mathbf{1}}\boldsymbol{\Gamma}_{\mathbf{s_{df}},\mathbf{2}:\mathbf{s_{df}}} \tag{24}$$

where

$$\boldsymbol{\Gamma}_{\mathbf{s_{df}},\mathbf{1}:\mathbf{s_{df}}-\mathbf{1}} = \boldsymbol{\Gamma}_{\mathbf{s_{df}}}(1:s_{\rm df}-1,:)$$
$$\boldsymbol{\Gamma}_{\mathbf{s_{df}},\mathbf{2}:\mathbf{s_{df}}} = \boldsymbol{\Gamma}_{\mathbf{s_{df}}}(2:s_{\rm df},:)$$

and † denotes the left-inverse.

As a result, the proposed subspace-aided approach for the frequency estimation can be summarized as follows:

Algorithm 2 Fundamental Frequency Identification

S1: Construct the Hankel matrices $\mathbf{D}_{\mathbf{s_{dp}},\mathbf{N}}$ and $\mathbf{D}_{\mathbf{s_{df}},\mathbf{N}}$ using measured periodic load $\mathbf{d}_k$.
S2: Perform the LQ decomposition and the SVD.
S3: Identify the matrix $\mathbf{A_d}$ in Eq.(24).
S4: Thus, the fundamental frequency of the unknown periodic load can be identified by the eigenvalue of $\mathbf{A_d}$ in Eq.(18).

IV. Robust Data-Driven Fault Detection Approach for the Drive Systems of Rolling Mills

In this section, a subspace-aided fault detection method with the unknown periodic load for the drive systems is proposed.

Based on the problem formulation in Section II-B, the input and output Hankel matrices can be denoted as $\mathbf{U}_{\mathbf{k},\mathbf{s},\mathbf{N}} \in \mathcal{R}^{\rm sl\times N}$ and $\mathbf{Y}_{\mathbf{k},\mathbf{s},\mathbf{N}} \in \mathcal{R}^{\rm sm\times N}$, and the extended state vector can be denoted as $\mathbf{X}_{\mathbf{k},\mathbf{1},\mathbf{N}} \in \mathcal{R}^{n_x\times N}$. Their forms are similar to that of the Hankel matrix for unknown periodic load in Section III-B. Then, the extended state-space representation of the drive systems in (2) and (3) can be formulated as

$$\mathbf{Y}_{\mathbf{k},\mathbf{s},\mathbf{N}} = \boldsymbol{\Gamma}_{\mathbf{s}}\mathbf{X}_{\mathbf{k},\mathbf{1},\mathbf{N}} + \mathbf{H}_{\mathbf{u},\mathbf{s}}\mathbf{U}_{\mathbf{k},\mathbf{s},\mathbf{N}} + \mathbf{H}_{\mathbf{d},\mathbf{s}}\mathbf{D}_{\mathbf{k},\mathbf{s},\mathbf{N}} + \mathbf{H}_{\boldsymbol{\alpha},\mathbf{s}}\boldsymbol{\Psi}_{\mathbf{k},\mathbf{s},\mathbf{N}} \tag{25}$$

where $\mathbf{H}_{\mathbf{d},\mathbf{s}}\mathbf{D}_{\mathbf{k},\mathbf{s},\mathbf{N}}$ denotes the sequence of periodic load. $\mathbf{H}_{\boldsymbol{\alpha},\mathbf{s}}\boldsymbol{\Psi}_{\mathbf{k},\mathbf{s},\mathbf{N}}$ denotes the noise sequence in which $\boldsymbol{\Psi}_{\mathbf{k},\mathbf{s},\mathbf{N}}$ consists of the noise vector $\boldsymbol{\alpha}_k$, and the structures of $\mathbf{H}_{\boldsymbol{\alpha},\mathbf{s}}$ and $\mathbf{H}_{\mathbf{u},\mathbf{s}}$ are similar. $\boldsymbol{\Gamma}_{\mathbf{s}}$ is the extended observability matrix and $\mathbf{H}_{\mathbf{u},\mathbf{s}}$ depicts the lower triangle block-Toeplitz matrix

$$\boldsymbol{\Gamma}_{\mathbf{s}} = \begin{bmatrix} \mathbf{C} \\ \mathbf{CA} \\ \vdots \\ \mathbf{CA}^{s-1} \end{bmatrix}, \mathbf{H}_{\mathbf{u},\mathbf{s}} = \begin{bmatrix} \mathbf{D} & \mathbf{0} & \cdots & \mathbf{0} \\ \mathbf{CB} & \mathbf{D} & \cdots & \mathbf{0} \\ \vdots & \vdots & \ddots & \vdots \\ \mathbf{CA}^{s-2}\mathbf{B} & \mathbf{CA}^{s-3}\mathbf{B} & \cdots & \mathbf{D} \end{bmatrix}.$$

According to LQ decomposition, assume the control loop is internally stable, a new data $\mathbf{M}_{\mathbf{k},\mathbf{s},\mathbf{N}}$ can be expressed as

$$\begin{aligned} \mathbf{M}_{\mathbf{k},\mathbf{s},\mathbf{N}} &= \mathbf{U}_{\mathbf{k},\mathbf{s},\mathbf{N}} + \mathbf{H}_{\mathbf{u},\mathbf{s}}\mathbf{Y}_{\mathbf{k},\mathbf{s},\mathbf{N}} \\ &= \boldsymbol{\Gamma}^{\mathbf{c}}_{\mathbf{s}}\mathbf{X}^{\mathbf{c}}_{\mathbf{k},\mathbf{1},\mathbf{N}} + \mathbf{H}^{\mathbf{c}}_{\mathbf{u},\mathbf{s}}\mathbf{W}_{\mathbf{k},\mathbf{s},\mathbf{N}} \end{aligned} \tag{26}$$

where the Hankel matrix $\mathbf{W}_{\mathbf{k},\mathbf{s},\mathbf{N}}$ is formed by the tracking reference $\boldsymbol{\omega}_k \in \mathcal{R}^m$. The matrices $\boldsymbol{\Gamma}^{\mathbf{c}}_{\mathbf{s}}$ and $\mathbf{H}^{\mathbf{c}}_{\mathbf{u},\mathbf{s}}$ consist of the system matrices of $\mathbf{K}(z)$

$$\mathbf{M}_{\mathbf{p},\mathbf{N}} = \mathbf{U}_{\mathbf{p},\mathbf{N}} + \mathbf{H}^{\mathbf{c}}_{\mathbf{u},\mathbf{s_p}}\mathbf{Y}_{\mathbf{p},\mathbf{N}} \in \mathcal{R}^{s_p l\times N}$$
$$\mathbf{M}_{\mathbf{f},\mathbf{N}} = \mathbf{U}_{\mathbf{f},\mathbf{N}} + \mathbf{H}^{\mathbf{c}}_{\mathbf{u},\mathbf{s_f}}\mathbf{Y}_{\mathbf{f},\mathbf{N}} \in \mathcal{R}^{s_f l\times N}$$
$$\mathbf{Z}_{\mathbf{c},\mathbf{p},\mathbf{N}} = \begin{bmatrix} \mathbf{U}^T_{\mathbf{p},\mathbf{N}} & \mathbf{Y}^T_{\mathbf{p},\mathbf{N}} \end{bmatrix}^T \in \mathcal{R}^{s_p(l+m)\times N}$$

where $\mathbf{D}_{\mathbf{b},\mathbf{N}}$ is the subspace of the unknown periodic load derived previously.

Due to the independence of future noise sequence, the Hankel matrix $\mathbf{Y}_{\mathbf{k},\mathbf{s},\mathbf{N}}$ could be orthogonally projected into different subspaces by an LQ decomposition so that to identify closed-loop data-driven SKR. Therefore, a subspace-aided fault detection method is summarized into the following theorem with considering the periodic load in the strip rolling process.

Theorem 1: As shown in Fig. 3, a standard feedback control loop which is composed of feedback controller $\mathbf{K}(z)$ in (4)–(5) and the drive system $\mathbf{G}(z)$ satisfies the following assumptions.

1) The controller $\mathbf{K}(z)$ is internally stable and the closed-loop is well-posed.
2) The reference signal $\boldsymbol{\omega}$ and the periodic load $\mathbf{d}_k$ are uncorrelated with the state vector $\mathbf{x}_k$ and the unknown noise $\boldsymbol{\alpha}_k$.
3) $s_f m > s_p(l+m)+(2n_f+1)$ and N are large enough to ensure that the matrix: $\mathbf{Z_{d,N}} = [\mathbf{Z}^T_{\mathbf{c,p,N}}\ \mathbf{D}^T_{\mathbf{b,N}}\ \mathbf{M}^T_{\mathbf{f,N}}\ \mathbf{Y}^T_{\mathbf{f,N}}]^T$ has full-row rank.

Thus, the thin LQ decomposition can be denoted as

$$\begin{bmatrix} \mathbf{Z_{c,p,N}} \\ \mathbf{D_{b,N}} \\ \mathbf{M_{f,N}} \\ \mathbf{Y_{f,N}} \end{bmatrix} = \underbrace{\begin{bmatrix} \mathbf{L_{c,11}} & \mathbf{0} & \mathbf{0} & \mathbf{0} \\ \mathbf{L_{c,21}} & \mathbf{L_{c,22}} & \mathbf{0} & \mathbf{0} \\ \mathbf{L_{c,31}} & \mathbf{L_{c,32}} & \mathbf{L_{c,33}} & \mathbf{0} \\ \mathbf{L_{c,41}} & \mathbf{L_{c,42}} & \mathbf{L_{c,43}} & \mathbf{L_{c,44}} \end{bmatrix}}_{\mathbf{L_c}} \underbrace{\begin{bmatrix} \mathbf{Q_{c,1}} \\ \mathbf{Q_{c,2}} \\ \mathbf{Q_{c,3}} \\ \mathbf{Q_{c,4}} \end{bmatrix}}_{\mathbf{Q_c}}$$

then a data-driven SKR $\mathcal{K}_{\mathbf{d,s_f}} \in \mathcal{R}^{n_\mathcal{K} \times s_f(l+m)}$ can be described as

$$\begin{aligned} \mathcal{K}_{\mathbf{d,s_f}} &= \left[\, \mathcal{K}_{\mathbf{u,s_f}}\ \mathcal{K}_{\mathbf{y,s_f}} \,\right] \\ \mathcal{K}_{\mathbf{u,s_f}} &= \mathcal{K}_{\mathbf{c,m,s_f}} \\ \mathcal{K}_{\mathbf{y,s_f}} &= \mathcal{K}_{\mathbf{c,y,s_f}} + \mathcal{K}_{\mathbf{c,m,s_f}} \mathbf{H^c_{u,s_f}} \end{aligned} \tag{27}$$

where

$$\left[\, \mathcal{K}_{\mathbf{c,m,s_f}}\ \mathcal{K}_{\mathbf{c,y,s_f}} \,\right] \begin{bmatrix} \mathbf{L_{c,31}} & \mathbf{L_{c,32}} & \mathbf{L_{c,33}} \\ \mathbf{L_{c,41}} & \mathbf{L_{c,42}} & \mathbf{L_{c,43}} \end{bmatrix} = \mathbf{0}. \tag{28}$$

Proof: The detailed proof is similar to that shown in [18], which is not enumerated here. ∎

Remark 1: $\mathcal{K}_{\mathbf{y,s_f}}$ is a part of the parity subspaces of the system with the length s_f, that is, $\mathcal{K}_{\mathbf{y,s_f}} \boldsymbol{\Gamma}_{\mathbf{s_f}} = \mathbf{0}$. If $\mathbf{D_{b,N}}$ is determined though the fundamental frequency of the unknown periodic load, a robust data-driven fault detection approach can be realized through $\mathcal{K}_{\mathbf{d,s_f}}$.

Then, a robust residual generator can be achieved by using the data-driven SKR $\mathcal{K}_{\mathbf{d,s_f}}$

$$\mathbf{r}_{\mathbf{d},k} = \mathcal{K}_{\mathbf{d,s_f}} \begin{bmatrix} \mathbf{u_{s_f,k}} \\ \mathbf{y_{s_f,k}} \end{bmatrix} \tag{29}$$

which can be rewritten as

$$\mathbf{r}_{\mathbf{d},k} = \boldsymbol{\epsilon}_k + \mathbf{f}_k, \quad \mathbf{f}_k = \begin{cases} 0 : \text{fault-free} \\ \neq 0 : \text{faulty} \end{cases} \tag{30}$$

where $\boldsymbol{\epsilon}_k \in \mathcal{N}(0, \Sigma_r)$ with the covariance matrix Σ_r. The following algorithms can solve the problem of detecting changes in $\mathbf{f}_k$. First, the threshold can be set by Algorithm 3.

Algorithm 3 Offline Setting

S1: Determine $\mathcal{X}_\alpha$ using the table of $\mathcal{X}^2$-distribution with one degree of freedom

$$prob\{\mathcal{X} > \mathcal{X}_\alpha\} = \alpha \tag{31}$$

where prob $\{\mathcal{X} > \mathcal{X}_\alpha\}$ denotes the probability of $\mathcal{X} > \mathcal{X}_\alpha$.
S2: Set threshold $J_{th} = \mathcal{X}_\alpha/2$.

Algorithm 4 Online Fault Detection Algorithm

S1: Collect online residual $\mathbf{r_{d},}_k$ in equation (29) which is achieved by using data-driven SKR.
S2: Set a window width k_w. Then, calculate the sum of residuals in each window,

$$\mathbf{r}_{\mathbf{d},win}(w) = \sum_{k=k_1}^{k_1+k_w-1} \mathbf{r}_{\mathbf{d},k}. \tag{32}$$

S3: Define the testing statistic

$$J = \frac{1}{2\Sigma_r k_w} \left(\sum_{w=1}^{N-k_w+1} \mathbf{r}^T_{\mathbf{d},win}(w) \mathbf{r}_{\mathbf{d},win}(w) \right). \tag{33}$$

where Σ_r is the covariance matrix of ϵ_k, N is the matrix length.
S4: Define the detection logic

$$\begin{cases} J \le J_{th} : \text{no fault}, \\ J > J_{th} : \text{faulty and alarm}. \end{cases} \tag{34}$$

V. Benchmark Study

For verifying the effectiveness of the proposed methods, this section is divided into two parts: numerical simulation and experimental verification. In experimental verification, the experimental data of the test rig for the drive systems of strip rolling mills is used.

A. Numerical Simulation

In the numerical simulation, a numerical example of a motor control system is given to verify Algorithm 1 and Remark 1. The variance of the noise sequence is set to be $P_{\alpha_i} = 0.001$ for $i = 1, \ldots, n_\alpha$. The length N is assumed to be 10^4. The sampling time of periodic load is $t_s = 0.01$ s. Furthermore, the fundamental frequency ω_0 is identified by measuring the output of the drive system and using Algorithm 2, which is consistent with the fundamental frequency of the original periodic load, that is, 0.1 Hz.

To verify the validity of Algorithm 1, the similarity between the real pulse wave and the subspace of the unknown periodic load constructed by different number of frequencies is shown in Fig. 5. The similarity is calculated as $(1 - (\|\mathbf{D_{f,N}} - \mathbf{D_{f,N}}\Pi_{\mathbf{D_{b,N}}}\|_2 / \|\mathbf{D_{f,N}}\|_2)) \times 100\%$, where the Hankel matrix $\mathbf{D_{f,N}}$ has the same structure as $\mathbf{U_{f,N}}$, and $\mathbf{D_{f,N}}\Pi_{\mathbf{D_{b,N}}}$ denotes the operator that projects the matrix $\mathbf{D_{f,N}}$ onto the subspace $\mathbf{D_{b,N}}$. In particular, the number of frequencies n_f depends on the practice.

Then, Algorithm 4 is given to compute the online residual evaluation and make a decision.

Fig. 6 shows the effectiveness of Remark 1 which describes the relationship between the nuclear norm of $\mathbf{P_{sf}}$ and the number of frequencies n_f. $\mathbf{P_{sf}}$ denotes the product of a part of kernel and the observability matrix $\mathbf{P_{sf}} = \mathcal{K}_{\mathbf{y,s_f}} \boldsymbol{\Gamma}_{\mathbf{s_f}}$. From Fig. 6, it can be concluded that as the number of frequencies n_f increases, the closer $\mathbf{P_{sf}}$ is to zero, the more accurate $\mathcal{K}_{\mathbf{y,s_f}}$ is identified.

B. Experimental Verification

To demonstrate the subspace-aided fault detection method, the experimental verification is implemented by the

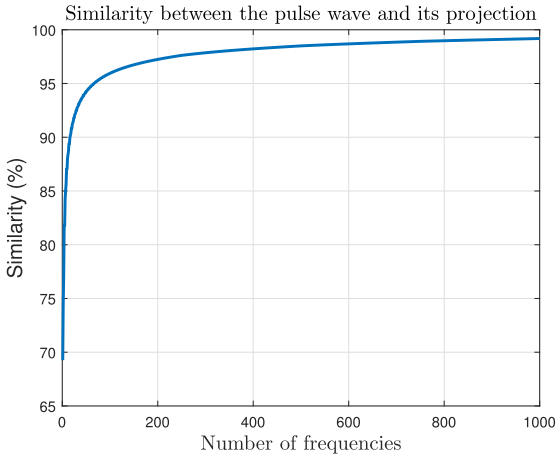

Fig. 5. Similarity between the constructed load and the real load.

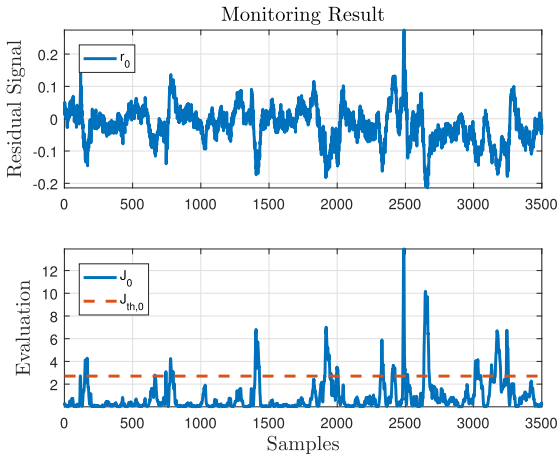

Fig. 7. Monitoring result without consideration of periodic load.

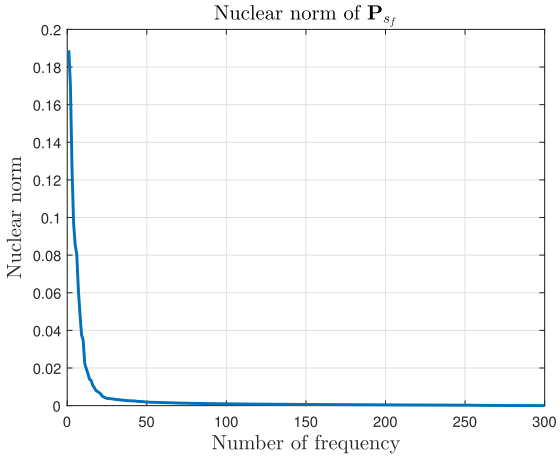

Fig. 6. Nuclear norm of $\mathbf{P_{sf}}$.

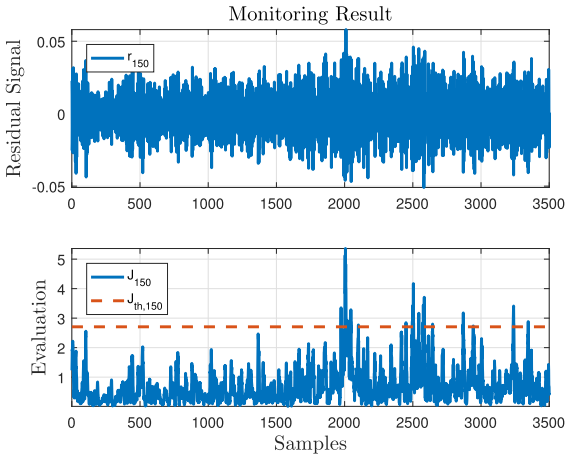

Fig. 8. Monitoring result with periodic load constructed by $n = 150$.

experimental data of the test rig for the drive systems of strip rolling mills.

The periodic load generated by the strip rolling process can directly affect the speed of drive systems as shown in Fig. 2. The process data is collected for validation. The reference of the drive system speed is 3000 rpm and the sampling time is set to be 0.01 s. The lengths of sp, sf, and N are chosen to be 20, 450, and 4000, respectively. During the operational status of the drive system, an actuator fault is occurred with a power reduction of 20% at the 2000th sampling instant. For the threshold setting, the fault alarm rate is chosen as $\alpha = 2\%$ in (31). In Algorithm 3, the window width is selected to be $k_w = 5$.

The monitoring result by traditional subspace identification method without consideration of the periodic load is shown in Fig. 7. The periodicity of residual is obvious and the existence of the periodic load affects the judgment. As can be seen from Fig. 7, the online evaluation approaches is close to or even exceeds the threshold before the fault occurs.

Meanwhile, the monitoring result by the proposed method considering periodic load which is constructed by 150 frequencies is shown in Fig. 8. As the number of frequencies n_f increases, the constructed periodic load becomes more and more accurate. As can be seen from Fig. 8, the periodic load is largely decoupled, and the periodicity of the residual is almost invisible. The residual can avoid the impact of the periodic load on the process monitoring. By comparing Figs. 7 and 8, the results show that the proposed approach can avoid the impact of the periodic load during the strip rolling process and detect the fault of the drive systems more effectively.

A quantile–quantile plot (Q–Q plot) shows the comparison of the quantile values of the data with the theoretical quantile values from a normal distribution. In the Q-Q plot, the reference line connects the first and third quartiles of the data, which is from the theoretical distribution. The degree of proximity to the normal distribution of the residuals from the two results above is tested in Fig. 9, which shows the Q–Q plot of the quantile values of the two residuals. In Fig. 9, the red lines are the reference lines for the no-fault residuals in Figs. 7 and 8. The black line is the quantile values of the no-fault residual in Fig. 7. In this case, the residual contains the whole periodic load and noise. The green line is the quantile values of the no-fault residual in Fig. 8, that is, the residuals after constructing the unknown periodic load with 150 frequencies. As can be seen from the figure, the green line is closer to its reference line than the black line and is almost coincides with its reference line, which indicates that the residual in Fig. 8 is almost normally distributed, and most of

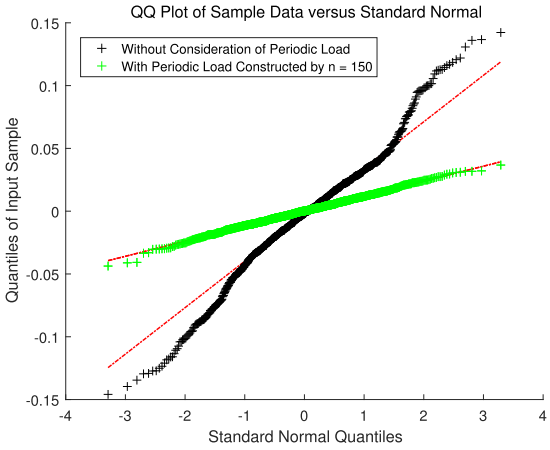

Fig. 9. Distribution of residuals between without consideration of periodic load and with periodic load constructed by $n = 150$.

the load is reconstructed and projected into the subspace $\mathbf{D_{b,N}}$. As can be seen from above, the unknown periodic load can be constructed accurately by Algorithm 1 so that the residual generation is robustness, which avoids the influence of the periodic load and is conductive to fault detection.

The above reliable results prove that the proposed fault detection method in this brief can be used to effectively detect the fault in the drive systems of strip rolling mills.

VI. Conclusion

In this brief, a subspace-aided fault detection approach is proposed for the drive systems of strip rolling mills. Considering the unknown periodic load in the drive system generated by the strip rolling process, a subspace description approach and a fundamental frequency identification approach for the unknown periodic load are proposed. The approaches are verified by the numerical example and the experimental data in the test rig for the drive systems of strip rolling mills. Compared with the traditional approaches which do not consider the unknown periodic load because of unmeasurable, the proposed approach can reduce the periodicity of the residual. The experimental results show that the proposed approaches have a better robustness on the unknown periodic load in the drive systems and avoid the impact on the fault detection rate of the drive systems during the strip rolling process and have practical application value.

References

[1] L. Chiang, E. Russell, and R. Braatz, *Fault Detection and Diagnosis in Industrial Systems*. London, U.K.: Springer, 2001.

[2] S. J. Qin, "Statistical process monitoring: Basics and beyond," *J. Chemometrics*, vol. 17, nos. 8–9, pp. 480–502, Aug. 2003.

[3] Z. Ge and J. Chen, "Plant-wide industrial process monitoring: A distributed modeling framework," *IEEE Trans. Ind. Informat.*, vol. 12, no. 1, pp. 310–321, Feb. 2016.

[4] H. Chen, B. Jiang, and N. Lu, "A newly robust fault detection and diagnosis method for high-speed trains," *IEEE Trans. Intell. Transp. Syst.*, vol. 20, no. 6, pp. 2198–2208, Jun. 2019.

[5] Z. Chen *et al.*, "A just-in-time-learning-aided canonical correlation analysis method for multimode process monitoring and fault detection," *IEEE Trans. Ind. Electron.*, vol. 68, no. 6, pp. 5259–5270, Jun. 2021.

[6] H. Ji, X. He, J. Shang, and D. Zhou, "Incipient fault detection with smoothing techniques in statistical process monitoring," *Control Eng. Pract.*, vol. 62, pp. 11–21, May 2017.

[7] C. Cheng, J. Wang, H. Chen, Z. Chen, H. Luo, and P. Xie, "A review of intelligent fault diagnosis for high-speed trains: Qualitative approaches," *Entropy*, vol. 23, no. 1, p. 1, Dec. 2020.

[8] C. Cheng, X. Qiao, B. Zhang, H. Luo, Y. Zhou, and H. Chen, "Multiblock dynamic slow feature analysis-based system monitoring for electrical drives of high-speed trains," *IEEE Trans. Instrum. Meas.*, vol. 70, pp. 1–10, 2021. [Online]. Available: https://ieeexplore.ieee.org/abstract/document/9393956

[9] Z. Gao, C. Cecati, and S. X. Ding, "A survey of fault diagnosis and fault-tolerant techniques—Part I: Fault diagnosis with model-based and signal-based approaches," *IEEE Trans. Ind. Electron.*, vol. 62, no. 6, pp. 3757–3767, Jun. 2015.

[10] S. X. Ding, P. Zhang, A. Naik, E. L. Ding, and B. Huang, "Subspace method aided data-driven design of fault detection and isolation systems," *J. Process Control*, vol. 19, no. 9, pp. 1496–1510, Oct. 2009.

[11] S. Ding, Y. Yang, and Y. Zhang, "Data-driven realizations of kernel and image representations and their application to fault detection and control system design," *Automatica*, vol. 50, no. 10, pp. 2615–2623, 2014.

[12] S. Ding, *Data-Driven Design of Fault Diagnosis and Fault-Tolerant Systems*. New York, NY, USA: Springer, 2014.

[13] S. Yin, H. Luo, and S. X. Ding, "Real-time implementation of fault-tolerant control systems with performance optimization," *IEEE Trans. Ind. Electron.*, vol. 61, no. 5, pp. 2402–2411, May 2014.

[14] H. Luo, S. Yin, T. Liu, and A. Khan, "A data-driven realization of the control-performance-oriented process monitoring system," *IEEE Trans. Ind. Electron.*, vol. 67, no. 1, pp. 521–530, Jan. 2020.

[15] S. Yin, H. Gao, J. Qiu, and O. Kaynak, "Fault detection for nonlinear process with deterministic disturbances: A just-in-time learning based data driven method," *IEEE Trans. Cybern.*, vol. 47, no. 11, pp. 3649–3657, Nov. 2017.

[16] Z. Chen, S. X. Ding, H. Luo, and K. Zhang, "An alternative data-driven fault detection scheme for dynamic processes with deterministic disturbances," *J. Franklin Inst.*, vol. 354, no. 1, pp. 556–570, 2017.

[17] H. Luo, K. Li, O. Kaynak, S. Yin, and H. Zhao, "A robust data-driven fault detection approach for rolling mills with unknown roll eccentricity," *IEEE Trans. Control Syst. Technol.*, vol. 28, no. 6, pp. 2641–2648, Nov. 2020.

[18] M. Huo, H. Luo, S. Yin, and O. Kaynak, "A data-driven fault detection approach for periodic rectangular wave disturbance," in *Proc. 44th Annu. Conf. IEEE Ind. Electron. Soc. (IECON)*, Washington DC, USA, Oct. 2018, pp. 6217–6222.

[19] P. John and A. S. Marwan, *Tandem Cold Metal Rolling Mill Control Using Practical Advanced Methods*. London, U.K.: Springer, 2011.

[20] L. Li, *Fault Detection and Fault-Tolerant Control for Nonlinear Systems*. Wiesbaden, Germany: Springer Vieweg, 2016.

[21] G. Vinnicombe, *Uncertainty Feedback: H_∞ Loop-Shaping ν-gap Metric*. London, U.K.: Imperial College Press, 2001.

[22] S. Smith, *The Scientist and Engineer's Guide to Digital Signal Processing*, 2nd ed. San Diego, CA, USA: California Technical Publishing, 1999.

[23] R. J. Beerends, H. G. ter Morsche, J. C. van den Berg, and E. M. van de Vrie, *Fourier and Laplace Transforms*. Cambridge, U.K.: Cambridge Univ. Press, 2003.